ARTICLE Thermophysics & Energy

OPEN ACCESS

Thermoelectric-based battery thermal management with cooling and energy recovery

Ding Luo,[1,2] Li Jiang,[1] Hao Chen,[1,*] Zihao Wu,[1] and Bingyang Cao[2,*]

[1]Shaanxi Key Laboratory of New Transportation Energy and Automotive Energy Saving, School of Energy and Electrical Engineering, Chang'an University, Xi'an 710064, China

[2]Key Laboratory for Thermal Science and Power Engineering of Ministry of Education, Department of Engineering Mechanics, Tsinghua University, Beijing 100084, China

*Correspondence: chenhao@chd.edu.cn (H. C.); caoby@tsinghua.edu.cn (B. C.)

Received: April 29, 2025; Accepted: September 19, 2025; Published Online: January 9, 2026; https://doi.org/10.59717/j.xinn-energy.2026.100134

Citation: Luo D., Jiang L., Chen H., et al. (2026). Thermoelectric-based battery thermal management with cooling and energy recovery. *The Innovation Energy* **3**:100134.

This work proposes the hybrid battery thermal management system (BTMS) integrating thermoelectric modules (TEM), phase change materials (PCM), and liquid cooling (LC) to achieve dual functionalities of TEM: power generation and cooling. A multi-physics numerical model is established to analyze the system's performance under varying discharge rates, along with proposing a phase transition temperature-triggered operational strategy. Results demonstrate that under 1 C to 4 C discharge conditions, the passive cooling system maintains the T_{max} of batteries below 323.15 K with a ΔT under 5 K, while TEM acts as the thermoelectric generator (TEG) to recover waste heat, exhibiting significant increases in output voltage and power with rising discharge rates. At 5C discharge, thermoelectric cooling (TEC) and LC reduce the T_{max} of batteries from 323.74 K to 321.51 K, while LC lowers the TEC hot-side temperature, thereby decreasing system energy consumption. The proposed 340 s delayed activation strategy for active cooling extends TEG power generation time by 340 s and reduces active cooling operation time by 47.2%. In 1C, 2C, 3C, and 4C discharge rates, the peak net energies of 22.15 J, 52.24 J, 53.60 J, and 41.93 J occur at liquid cooling mass flow rates of 0.3 g/s, 0.5 g/s, 0.7 g/s, and 0.7 g/s, respectively. This work provides an innovative solution for the BTMS that balances thermal control efficiency and energy recovery.

INTRODUCTION

To address the economic and environmental issues caused by the excessive consumption of traditional fossil fuels, the promotion of electric vehicles has become a critical solution in the transportation sector.[1,2] According to the International Energy Agency's report, the demand for electric vehicles has surged, and battery demand is expected to continue rising, potentially reaching 4.5 times the current level by 2030.[3] Lithium-ion batteries are widely used in the field of electric vehicles due to their high energy density, high voltage output, and flat discharge characteristics.[4] However, lithium-ion batteries face thermal safety issues, as excessively high temperatures can reduce their performance and lifespan, and even trigger thermal runaway; excessively low temperatures can lead to capacity degradation and internal short circuits.[5,6] The ideal operating temperature of lithium-ion batteries should be maintained within the range of 293.15 to 323.15 K,[7] and the temperature difference within the battery module should be controlled to within 5 K.[8] Therefore, it is essential to develop an effective battery thermal management system (BTMS) to control the operating temperature of lithium-ion batteries.

Battery thermal management technologies mainly include air cooling (AC), liquid cooling (LC), phase change material (PCM) cooling, heat pipe (HP) cooling, and thermoelectric cooler (TEC) cooling. Among these, PCMs show great potential due to their cost-effectiveness, excellent thermal consistency, and outstanding heat dissipation performance.[9] Research has shown that PCMs can not only effectively reduce the maximum operating temperature of the battery but also significantly improve the uniformity of temperature distribution.[10] However, the low thermal conductivity and limited latent heat capacity of PCMs remain the main bottlenecks in practical applications. To enhance the thermal conductivity of PCMs, materials with high thermal conductivity, such as graphite or metal particles, are typically integrated to facilitate internal heat transfer, thereby improving their thermal management capability.[11,12] For example, Ping et al.[13] developed a novel composite PCM and studied its application performance in the BTMS. Experimental results show that the material exhibits excellent cooling performance, reducing the peak battery temperature by 23.7% under 3C high-rate discharge conditions, while maintaining the temperature difference within 3 K. Masthan et al.[14] added carbon-based material of graphite powder to paraffin to improve thermal conductivity. Experimental results show that at all discharge rates, the CPCM with a hexagonal battery pack has demonstrated good performance by keeping its temperature below 323.15 K. Furthermore, HPs possess high thermal transfer efficiency, and combining PCMs with HPs can effectively overcome the low thermal conductivity and heat accumulation issues of PCMs. For example, Abd et al.[15] studied the BTMS with flat HPs coupled with PCMs. Under an ambient temperature of 308.15 K and a 3 C discharge condition, the maximum battery operating temperature of the HP-coupled PCM system is reduced by 21.1% compared to the system using only PCMs. However, due to the limited latent heat capacity of PCMs, PCMs may not be able to effectively cool the battery under complex operating conditions. Therefore, PCMs often need to be combined with additional cooling technologies to dissipate the absorbed heat promptly. AC combined with PCMs can delay the melting process of the PCM, thereby maintaining the battery within the optimal operating temperature range.[16] However, the air has a limited heat-carrying capacity due to its lower specific heat capacity, while LC can dissipate heat more effectively and rapidly restore the latent heat storage capacity of PCMs by accelerating their solidification.[17] Additionally, combining PCMs with TEC can effectively regulate the battery temperature and prolong the melting time of PCMs, thereby maximizing their effectiveness.[18] Luo et al.[19] introduced the concept of latent heat recovery rate for PCMs and demonstrated that the incorporation of TEC not only significantly improves latent heat recovery efficiency but also enables high-temperature cooling of the battery.

TEC operates based on the Peltier effect, where heat is absorbed or released at its two ends when current flows, thereby achieving battery cooling. In contrast, thermoelectric modules (TEMs) based on the Seebeck effect generate a voltage when a temperature difference exists across their ends, and this principle can be used as the energy conversion mechanism in thermoelectric generators (TEGs).[20] However, recent reviews indicate that in PCM-TEC hybrid systems, TEMs are typically used solely for unidirectional cooling,[9] with neither TEG mode nor dual-function switching being considered. Researches on the application of the TEG in the BTMS and its power generation performance is still insufficient. Jiang et al.[21] found that under a battery heating power of 6 W, the PCM-only passive cooling module required 930 s to raise the battery temperature to 323.15 K; with the addition of the TEC, this duration was extended to 5335 s. Therefore, when the passive thermal management system of the hybrid BTMS can meet the cooling requirements, the TEM does not need to operate continuously as a TEC and possesses the potential to generate power as a TEG. Furthermore, whether TEMs are used as TECs or TEGs, the BTMS involves the coupling of heat transfer, electric, and flow fields, requiring the establishment of an accurate numerical model for performance analysis.

Therefore, this work presents a hybrid BTMS integrating PCM, TEM, and LC. The system leverages PCM's high latent heat absorption, LC's rapid heat dissipation, and the dual functionality of the TEM to ensure temperature control while recovering waste heat and enhancing overall energy efficiency. Based on the hybrid BTMS, this work develops a multiphysics-coupled numerical model to evaluate system performance. While prior studies leveraged TEMs solely as TECs or explored TEG principles, this work pioneers a dual-functional TEM regime. By dynamically switching between TEG and TEC modes triggered by PCM phase transition, the system simultaneously achieves waste heat recovery and on-demand cooling, establishing an energy-neutral thermal management framework. First, the thermal performance of

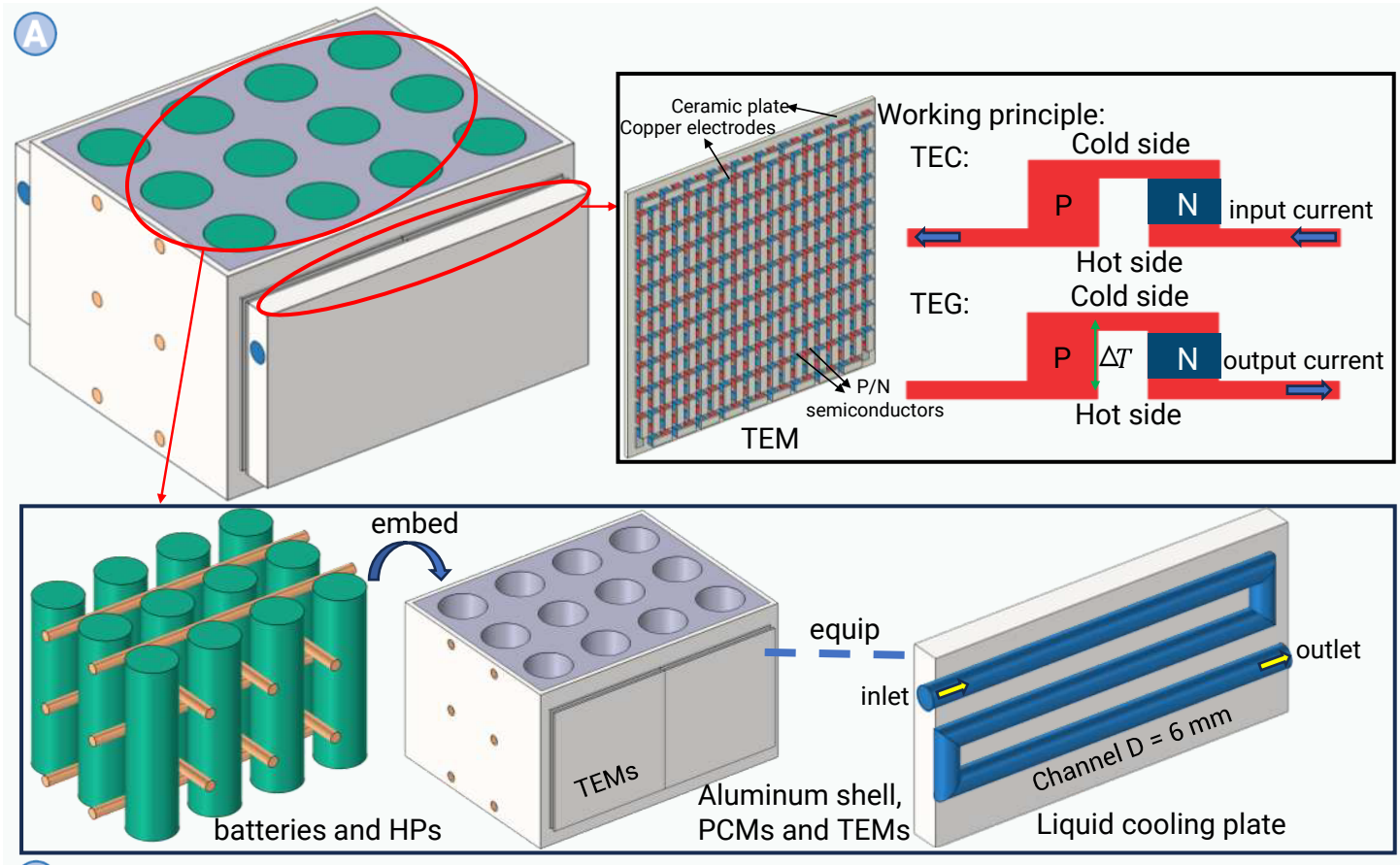

B

The heat generation rate of batteries at different discharge rates

Discharge rate (C)	1	2	3	4	5
Heat generation rate ($W \cdot m^{-3}$)	24277.22	68989.15	134135.79	2197717.13	325733.19

Figure 1. (A) Physical structure of the hybrid BTMS. (B) The heat generation rate of batteries at different discharge rates.

the passive cooling system is analyzed. When the passive cooling system meets the thermal management requirements, the TEM is employed as the TEG for power generation. Subsequently, when passive cooling proves inadequate, the thermal performance of systems with various active cooling components added is compared. Then, an operational strategy for the active cooling system is proposed to enable the TEM's dual functions of power generation and cooling, thereby reducing energy consumption while still satisfying thermal management requirements. Finally, the impact of LC mass flow rate on net energy is investigated.

MATERIALS AND METHODS

Structure of the hybrid BTMS

The proposed hybrid BTMS consists of cylindrical batteries, an aluminum shell, PCMs, HPs, TEMs, and liquid cooling plates, as shown in Figure 1A. The battery has a diameter of 18 mm and a height of 65 mm, arranged in three rows and four columns with a spacing of 8 mm. The aluminum shell has dimensions of 104 mm×78 mm×65 mm (length×width×height), with a wall thickness of 2 mm, and contains organic paraffin PCM with strong plasticity and ease of hole drilling, used to secure the batteries and HPs. The TEM (50 mm×50 mm×3.3 mm) is attached to the outer side of the aluminum shell, with its hot end equipped with a 100 mm×50 mm×8 mm liquid cooling plate that has a built-in S-shaped flow channel with a 6 mm diameter, using water as the coolant to enhance the temperature difference effect.[22] When the passive cooling system (PCMs and HPs) meets the thermal management needs, the TEM operates as a TEG; when the passive system cannot meet the demand, the TEM is powered to switch to TEC, working together to enhance heat dissipation. The system material parameters and characteristics are detailed in Table 1. The thermophysical parameters of the TEM are shown in Table 2.

Model development of the hybrid BTMS

To accurately analyze the performance of the hybrid BTMS and simplify the computational domain, the following assumptions are made:

(1). Only a thermal model of the battery is established to study its thermal behavior [26];

(2). The heat transfer process of the HP is simulated using the thermal physical properties of the HP material;[27]

(3). The simulation ignores the flow and density changes caused by phase transitions in the PCM.[28]

Computational domain

Heat transfer domain. During operation, the heat released by the battery is first absorbed by the PCM, causing its temperature to rise and triggering the phase change latent heat absorption process. The heat is then efficiently dissipated to the external environment through HPs and the aluminum shell while being transferred to the TEM. Moreover, during TEM operation, Peltier heat, Joule heat, and Thomson heat are generated. These intrinsic heat sources, along with the original heat flux from the battery, contribute to the complex heat transfer process. To maintain the efficient operation of the TEM, the accumulated heat on its hot side is rapidly dissipated through the liquid cooling plate. The above heat transfer process follows the energy conservation equation below:

Table 1. Material parameters and characteristics.

Property	Battery[23]	PCM[21]	Aluminum shell	Water	HPs[24]
Nominal capacity (Ah)	2.6	–	–	–	–
Nominal voltage (V)	3.7	–	–	–	–
Internal resistance (mΩ)	25	–	–	–	–
Density ($kg·m^{-3}$)	2720.59	850·	2700	998	8960
Heat capacity ($J·kg^{-1}·K^{-1}$)	1069.16	2000	900	4200	381
Thermal conductivity ($W·m^{-1}·K^{-1}$)	3.5	0.2	238	0.6	2000
Latent heat ($kJ·kg^{-1}$)	–	255	–	–	–
Phase transition temperature (K)	–	314.15-317.15	–	–	–

Table 2. Thermoelectric parameters of the TEM components.[25]

	Seebeck coefficient ($\mu V·K^{-1}$)	Thermal conductivity ($W·m^{-1}·K^{-1}$)	Electrical conductivity ($S·m^{-1}$)	Size (L·W·H mm^3)
n-type semiconductor	$3.217\times10^{-8}T^4$ $-4.587\times10^{-5}T^3$ $+2.385\times10^{-2}T^2$ $-5.531T+336.358$	$-1.107\times10^{-9}T^4$ $+1.786\times10^{-7}T^3$ $-1.050\times10^{-4}T^2$ $+0.2664T-23.684$	$-2.791\times10^{-5}T^4$ $+5.121\times10^{-2}T^3$ $-33.758T^2$ $+9.335\times10^3T-8.293\times10^5$	1.4×1.4×1
p-type semiconductor	$1.936\times10^{-8}T^4$ $-3.718\times10^{-5}T^3$ $+2.424\times10^{-2}T^2$ $-6.366T+772.024$	$1.802\times10^{-8}T^4$ $-2.863\times10^{-5}T^3$ $+1.794\times10^{-2}T^2$ $-5.198\times10^{-2}T+6.821$	$4.480\times10^{-8}T^4$ $-7.364\times10^{-7}T^3$ $+42.205\times10^{-2}T^2$ $-1.389\times10^2T+1.595\times10^6$	1.4×1.4×1
copper electrodes	–	400	5.998×10^7	3.8 × 1.4× 0.35
ceramic plates	–	$0.0286T+28.376$	–	50 × 50× 0.8

$$\frac{\partial}{\partial t}(\rho_x c_{p,x} T_x) = \nabla\cdot(k_x \nabla T_x) + \dot{S}_x \tag{1}$$

$$\dot{S}_x = \begin{cases} Q_b; battery \\ \sigma_p^{-1}(T_p)\vec{j}^{\,2} - \nabla a_p(T_p)\vec{J}T_p - \\ \quad \frac{\partial a_p(T_p)}{\partial T_p} T_p \vec{J}\cdot\nabla T_p; & p-type\ semiconductor \\ \sigma_n^{-1}(T_n)\vec{j}^{\,2} - \nabla a_n(T_n)\vec{J}T_n - \\ \quad \frac{\partial a_n(T_n)}{\partial T_n} T_n \vec{J}\cdot\nabla T_n; & n-type\ semiconductor \\ \sigma_{co}^{-1}(T_{co})\vec{j}^{\,2}; & copper\ electrode \\ 0; ceramic\ plate,\ HP,\ liquid & cooling\ palte \end{cases} \tag{2}$$

where ρ, c_p, T, k, σ, a, $\vec{j}$, represent density, specific heat capacity, temperature, thermal conductivity, electrical conductivity, Seebeck coefficient, and current density vector, respectively. The subscripts x, b, p, n, and co represent the material type, battery, p-type semiconductor, n-type semiconductor, and copper electrode, respectively. $\dot{S}$ represents the energy source term, and Q denotes the heat generation rate of the battery. Different battery discharge rates correspond to different volumetric heat generation rates, as shown in Figure 1B. Furthermore, this work employs a numerical model based on phase change enthalpy to analyze the PCM, accurately simulating the coupled heat transfer and phase change process by solving the differential term of phase change enthalpy in the energy conservation equation, as shown below:

$$\rho_{PCM}\frac{\partial H_{PCM}}{\partial t} = \nabla\cdot(k_{PCM}\nabla T_{PCM}) \tag{3}$$

$$H_{PCM} = \int_{T_{amb}}^{T_{PCM}} c_{p,PCM}\,dT + \beta L \tag{4}$$

$$\beta = \begin{cases} 0; T_{PCM} < T_s \\ \frac{T_{PCM}-T_s}{T_l-T_s}; T_s \le T_{PCM} < T_l \\ 1; T_{PCM} \ge T_l \end{cases} \tag{5}$$

where H_{pcm}, β, L denote the PCM enthalpy, the liquid fraction of the PCM, and latent heat, respectively. The subscripts s and l represent the solid and liquid state temperatures of the PCM, respectively. Equations (3)-(5) adopt a linear liquid-fraction assumption for computational efficiency in multi-physics coupling. This approach is validated for organic paraffin PCMs with solid-liquid interfaces.[15,28]

Electric domain. The thermoelectric conversion process in the TEM is achieved through both thermal conduction and electrical conduction. When a current is applied to the TEM, its two ends absorb or release heat, thereby enabling a cooling function; whereas when a temperature difference exists between the two ends, a voltage is generated. Therefore, in the electrical domain, the TEM must satisfy the conservation of electric potential, the relationship between current density and electric field strength, as well as the condition of current continuity, as shown below:

$$\vec{E} = -\nabla\varphi + a_x(T)\nabla T \tag{6}$$

$$\vec{J} = \sigma_x \vec{E} \tag{7}$$

$$\nabla\cdot\vec{J} = 0 \tag{8}$$

where $\vec{E}$ represents the vector density of the electric field, and φ denotes the electric potential.

Fluid domain. The fluid domain only involves the cooling water in the liquid cooling plate. First, the flow regime of the cooling water is determined based on the Reynolds number, which is defined as follows:

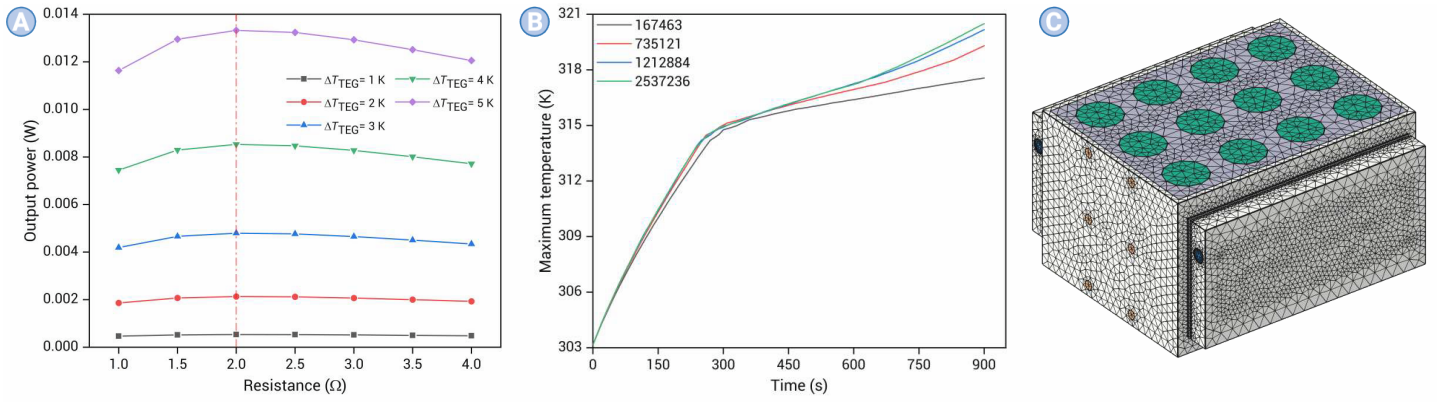

Figure 2. (A) Dependence of TEG internal resistance and output power on varying thermal gradients. (B) Impact of grid number on the battery's T_{max}. (C) Model nodes.

$$Re = \frac{\rho \vec{v} D}{\mu} \tag{9}$$

$$\vec{v} = \frac{4\dot{m}}{\rho \pi D^2} \tag{10}$$

where D and $\dot{m}$ represent the diameter of the flow channel and the mass flow rate, respectively. In this work, the maximum mass flow rate of the cooling water is 0.9 g/s, with a Reynolds number of 189.18, which is below 2300; therefore, the flow regime of the cooling water is determined to be laminar. The transient transport characteristics of the cooling water can be described based on Computational Fluid Dynamics theory, with the conservation equations of momentum, mass, and energy as follows:

$$\frac{\partial}{\partial t}(\rho \vec{v}) + \nabla \cdot (\rho \vec{v} \vec{v}) = -\nabla p + \nabla \cdot (\mu \nabla \vec{v}) \tag{11}$$

$$\frac{\partial \rho}{\partial t} + \nabla \cdot (\rho \vec{v}) = 0 \tag{12}$$

$$\frac{\partial (\rho c_p T)}{\partial t} + \nabla (\rho c_p \vec{v} T) = k \nabla^2 T \tag{13}$$

where p, μ, and $\vec{v}$ represent pressure, dynamic viscosity, and velocity vector, respectively.

Parameter definitions

This study characterizes the power generation performance of TEM when functioning as a TEG through instantaneous output power:

$$P(t) = \sum_1^n \frac{U^2(t)}{R} \tag{14}$$

where $U(t)$ represents the instantaneous terminal voltage of the TEG, R denotes the internal resistance of a single TEG, and n indicates the number of TEMs. As shown in Table 2, the parameters of thermoelectric materials are temperature-dependent, leading to variations in TEG internal resistance with temperature. To achieve maximum output power, it is necessary to investigate the internal resistance characteristics under different temperature gradients between the cold and hot ends, where power peaks occur when load resistance equals internal resistance. Accordingly, this paper investigates the power output characteristics of TEMs under 1-5 K temperature differences with varying load resistances. As shown in Figure 2A, the maximum output power occurs at 2 Ω load resistance. Therefore, a single TEM load resistance of 2 Ω is maintained throughout the simulations. Given the requirement to employ a liquid cooling system to reduce the hot-end temperature of TEMs, the instantaneous pump power is defined as:

$$P_{LC}(t) = \dot{m} \frac{\Delta p(t)}{\rho} \tag{15}$$

where $\dot{m}$ represents the coolant mass flow rate, $\Delta p(t)$ denotes the instantaneous pressure drop. Moreover, the input power of the TEC is defined as follows:[29]

$$P_{TEC}(t) = I_{TEC}^2(t) R_{TEC} + \alpha I_{TEC}(t) [T_h(t) - T_c(t)] \tag{16}$$

where P_{TEC}, I_{TEC}, and R_{TEC} represent the input power, input current, and resistance of the TEC, respectively, with the subscripts h and c denoting the hot and cold sides of the TEC. To emphasize the power generation advantage of TEGs in exploiting minimal temperature differences within the BTMS, a net output energy model is established as follows:

$$E = \int P(t) - P_{LC}(t) dt \tag{17}$$

Boundary conditions

The initial system temperature, ambient temperature, and cooling water temperature are all set to 303.15 K to simulate the operation of the BTMS under normal working conditions. Selecting the discharge rate range of 1 C-5 C covers typical battery operating scenarios from mild to high intensity loads. Specifically, 1-4 C denotes common usage conditions, while 5 C is used as a high discharge rate to evaluate the system's thermal performance under extreme loading. When operating as a TEC, the TEM is supplied with an input current of 0.5 A, whereas when functioning as a TEG, it generates an output voltage. The outlet pressure of the liquid cooling plate is set to 0, and the inlet boundary condition is defined by the mass flow rate, which ranges from 0 to 0.9 g/s in this work. All interfaces exposed to the external environment are defined as thermal loss interfaces, with heat loss governed by the following equation:

$$-k \frac{\partial T}{\partial n} = h_{amb} (T - T_{amb}) \tag{18}$$

where, $\frac{\partial T}{\partial n}$ represents the temperature gradient along the heat conduction direction, and h_{amb} denotes the ambient convective heat transfer coefficient, which is set to 5 W/(m^2·K).[5]

Grid independence

Using COMSOL, numerical calculations of the above equations are performed under specified boundary conditions and initial values to investigate the performance of the hybrid BTMS. The mesh size of the computational domain has a significant impact on both the accuracy and computational efficiency of the results. To improve computational efficiency and ensure accuracy, this work tests the maximum battery temperature during a 4 C discharge for the hybrid BTMS under different grid counts, as shown in Figure 2B. When the grid counts are 167463, 735121, 1212884, and 2537236 respectively, the maximum battery temperatures at the end of discharge are 317.56 K, 319.3 K, 320.17 K, and 320.49 K. Using the results obtained with a grid count of 2537236 as the benchmark, the absolute errors for mesh counts of 167463, 735121, and 1212884 are 0.91%, 0.37%, and 0.09%, respectively. The results indicate that the simulation outcomes tend to be stable when the grid count exceeds 1212884. Therefore, in the simulation of the hybrid BTMS, the grid count should be greater than 1212884, as shown in Figure 2C.

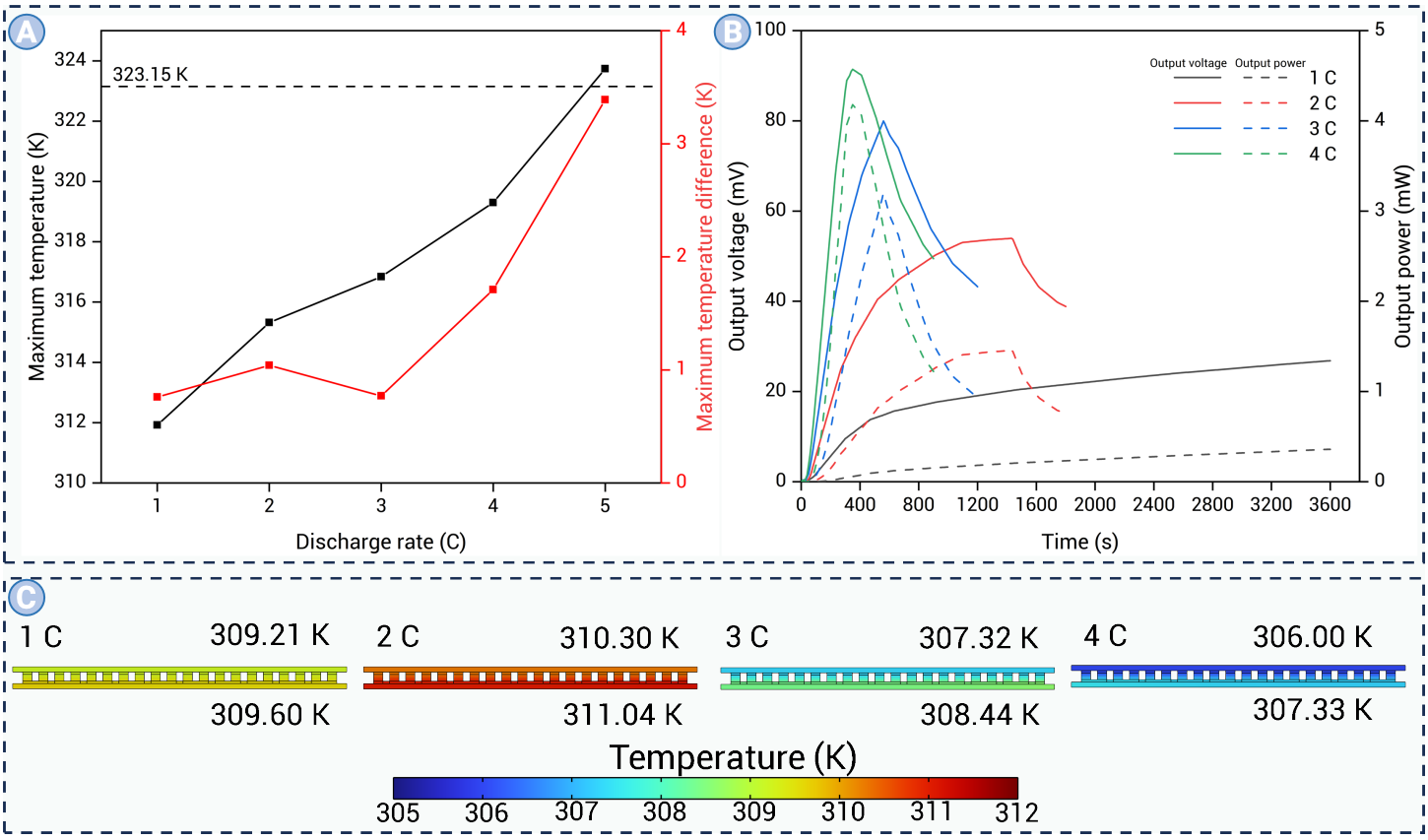

Figure 3. (A) Thermal performance of the system; (B) Performance of the TEG; (C) Temperature distribution characteristics at the cold/hot sides of the TEG.

Experimental validation

In a previous study,[19] the multiphysics numerical model used in this work was experimentally validated. Therefore, in this work, the experimental platform is not repeatedly built, but the validated simulation model is directly used for performance analysis. Specifically, under the conditions of a battery heat generation power of 6 W, a cooling water flow rate of 0.75 L/min, a PCM composed of copper foam-paraffin composite, and a TEC input current of 6.5 A, the simulation results closely match the experimental data. The mean absolute errors of the maximum temperature and temperature difference are 0.849 K and 0.183 K, respectively, both within an acceptable range, demonstrating that the numerical model can accurately assess the system's thermal performance.

RESULTS AND DISCUSSION

TEM acts as the TEG

In this TEM-based hybrid thermal management system, the presence of the passive cooling system composed of PCMs and HPs allows passive cooling to regulate battery temperature under certain conditions. At this point, if the TEM continues to function as the TEC, it will result in unnecessary energy consumption. Instead, the temperature difference generated by battery heat can be utilized to operate the TEM as the TEG, enabling energy recovery. Therefore, the thermal management capability of the passive cooling system is first investigated. Under these conditions, no operating current is supplied to the TEM, and the mass flow rate at the liquid cooling plate inlet is zero.

Figure 3A illustrates the variation characteristics of the maximum temperature (T_{max}) and maximum temperature difference (ΔT_{max}) of the battery under different discharge rates. The simulation results indicate that as the discharge rate increases, the T_{max} rises. At a 5 C discharge rate, the T_{max} of the battery exceeds 323.15 K, whereas at discharge rates between 1 C and 4 C, the T_{max} of the battery remains below 323.15 K. This indicates that the passive cooling system can effectively regulate battery temperature within the range of 1 C to 4 C, keeping it below 323.15 K. Additionally, the passive cooling system composed of PCM and HP ensures that under discharge rates from 1 C to 5 C, the ΔT_{max} of the battery remains below 5 K, maintaining excellent thermal uniformity. Within the 1-4 C discharge range, the PCM absorbs the heat released by the battery and undergoes phase change. Concurrently, a portion of the heat is dissipated externally via the HP, thereby delaying the rise in battery temperature. However, when the discharge rate increases to 5 C, the battery's heat generation rate increases significantly, and the heat dissipation capacity of both the PCM and HP cannot meet the thermal load, resulting in the battery temperature exceeding 323.15 K. In addition, the PCM uniformly absorbs the heat released by the battery throughout the discharge process, demonstrating excellent temperature equalization. Therefore, at discharge rates between 1 C and 4 C, thermal management can rely on the passive cooling system, allowing the TEM to function as the TEG and achieve thermoelectric power generation.

Figure 3B presents the output voltage and output power of the TEG under different discharge rates. The simulation results indicate that as the discharge rate increases, the output voltage and power of the TEG rise simultaneously, with higher discharge rates leading to greater peak values of voltage and power. Additionally, during the 1 C discharge process, the TEG's output voltage and power continuously increase, whereas during 2 C, 3 C, and 4 C discharges, the output voltage and the output power first rise and then decline. At a 1 C discharge rate, the battery's T_{max} is 311.92 K, which is below the PCM's phase change temperature range. The heat generated by the battery is transferred to the TEG through the PCM, causing the TEG's ΔT to increase continuously and, according to the thermoelectric coupling equations, the TEG's output voltage and power to rise accordingly. However, when the discharge rate increases to the 2 C - 4 C range, the battery temperature exceeds the PCM's phase-change window, thereby triggering the phase transition of the PCM. Before the phase transition, the heat released by the battery still transfers to the TEG, further increasing the TEG's ΔT and thus continuing to boost its output voltage and power. During the phase change process, the PCM absorbs substantial latent heat, which reduces the heat flux delivered to the TEG, lowers the ΔT, and consequently causes its output voltage and power to decline. Furthermore, the sequence of peak occurrences in TEG output voltage and power suggests that higher discharge rates

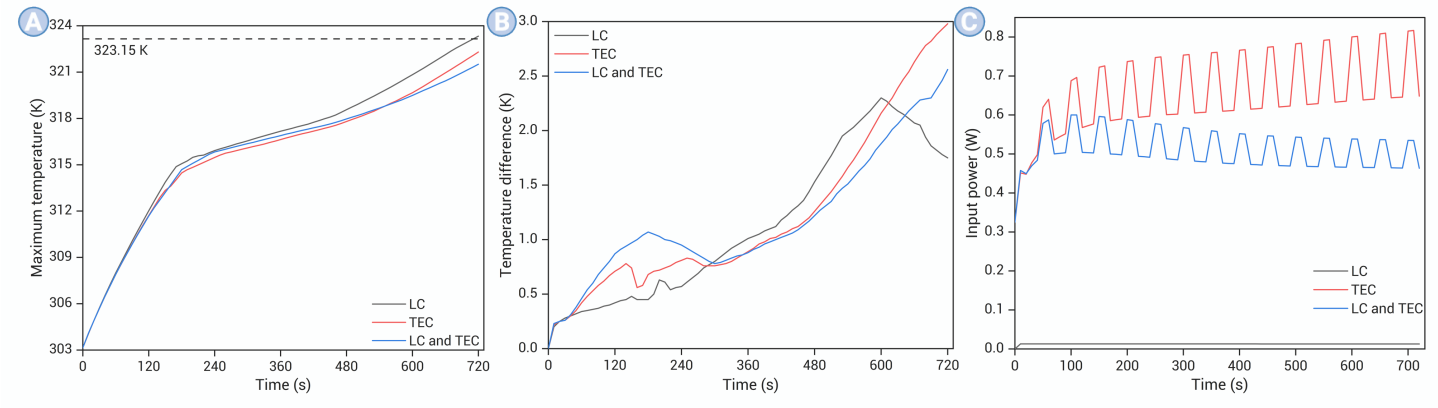

Figure 4. Performance of the system with different active cooling configurations: (A) T_{max} of the battery; (B) ΔT of the battery; (C) System input power.

lead to an earlier PCM phase change, causing the TEG's output voltage and power to decrease earlier.

Figure 3C illustrates the temperature characteristics when the TEG output voltage and power reach their maximum under different discharge rates. It can be observed that the greater the TEG's ΔT, the larger its output voltage and power. Under discharge rates from 1 C to 4 C, the peak values of the TEG' s output voltage and power gradually increase, corresponding to the TEG's ΔT of 0.39 K, 0.74 K, 1.12 K, and 1.33 K, respectively. Additionally, the peak values of output voltage and power correspond to the critical temperature of the PCM phase transition. Since heat must transfer from the high-temperature region to the low-temperature region, this process requires time, especially in PCM with relatively poor thermal conductivity. Therefore, the TEG's temperature response exhibits a delay, causing its temperature to remain lower than the PCM phase transition temperature of 314.15 K.

TEM acts as the TEC

Previous section indicates that when the discharge rate is between 1 C and 4 C, the passive cooling system alone can meet the thermal management requirements. However, at a discharge rate of 5 C, the passive cooling system is insufficient for effective thermal management, requiring additional cooling capacity from the active cooling system. In this hybrid BTMS, the active cooling system consists of the LC and the TEM operating as the TEC. To meet cooling demands while conserving energy, this section investigates the thermal performance and input power of the system under 5 C discharge conditions when LC, TEC, or both LC and TEC are added to the passive cooling system. At this time, the mass flow rate of the LC is 0.1 g/s, and the input current of the TEC is 0.5 A.

Figure 4A shows the variations in T_{max} of the battery after the incorporation of different active cooling systems. When LC, TEC, and both LC and TEC are employed, the T_{max} of the battery is 323.33 K, 322.3 K, and 321.51 K, respectively, all lower than the 323.74 K observed under the passive cooling system. However, when only LC is used, the T_{max} of the battery still exceeds 323.15 K, indicating that the cooling capacity of LC alone is insufficient. In contrast, the addition of TEC provides sufficient cooling. Moreover, by employing the LC to cool the hot side of the TEC, the battery's T_{max} is further reduced. This effect arises because LC-assisted cooling of the TEC hot side diminishes its ΔT; according to the TEC cooling power equation,[30] a reduced ΔT increases cooling power and thereby enhances overall thermal management performance. Figure 4B displays the variations in the battery's ΔT after the incorporation of various active cooling systems. Compared to the battery's ΔT_{max} With 3.39 K under only the passive cooling system, the incorporation of active cooling systems results in a more uniform temperature distribution. Specifically, with the incorporation of LC, TEC, and both LC and TEC, the ΔT_{max} of battery decreases to 1.75 K, 2.98 K, and 2.56 K, respectively.

Figure 4C illustrates the system's input power after the incorporation of various active cooling systems. The passive cooling system consumes no energy, so its input power is zero. With the addition of LC, the system's input power is solely that of the liquid cooling pump. Since the LC's mass flow rate remains constant during discharge and the pressure drop is relatively stable, its input power is approximately 0.01 W. With the addition of the TEC, the system's input power is that of the TEC. When the input current of the TEC is kept constant, according to Equation (16), its output power is jointly influenced by the material's internal resistance, Seebeck coefficient, and the ΔT. Since the internal resistance and Seebeck coefficient vary with temperature (as shown in Table 2), the TEC input power exhibits a sawtooth-like fluctuation around 0.7 W due to the combined influence of these parameters. Notably, when the LC is used in conjunction with the TEC, the total system input power exhibits sawtooth-like fluctuations around 0.5 W, which is significantly lower than when the TEC is used alone. This is because the liquid cooling system reduces the hot-side temperature of the TEC, thereby decreasing the ΔT between the hot and cold sides; according to Equation (16), a reduced ΔT leads to lower TEC input power. This reduction is greater than the additional power consumed by the LC during operation. Thus, the total system input power is reduced. In summary, the LC system assists in cooling the TEC by reducing its ΔT, thereby enhancing the thermal performance of the BTMS and lowering the overall system energy consumption.

An operational strategy to enable the TEM's dual functions

When the battery discharge rate is 5 C, the passive cooling system alone is insufficient for thermal management, necessitating the incorporation of the TEC. However, the TEC requires an input current to operate, consuming a significant amount of energy. Previous section demonstrates that the synergy between the TEC and LC can reduce system energy consumption. To further enhance energy efficiency, this section proposes an operational strategy for the active cooling system: activating the system at a specific time point after the battery begins discharging. Before activation, the TEM functions as the TEG for power generation; After activation, it operates as the TEC to manage the battery's thermal conditions. This strategy enables TEG power generation while also reducing the operational duration of the TEC and LC, thereby conserving energy. In studies on the thermal degradation mechanism of PCM-based hybrid BTMS, the optimal activation time is considered to be when the battery temperature reaches the upper limit of the PCM phase change temperature.[31] In our previous study,[32] this strategy is proven to ensure that the system's thermal performance meets the required standards while minimizing the active cooling operation time, thereby extending the TEG power generation duration. In this study, under a 5C discharge rate with only the passive cooling system, the battery temperature reaches the phase change temperature limit at 340 s. Therefore, before 340 s of discharge, the TEM functions as the TEG to generate power from a minor temperature difference. At 340 s, the TEC and LC are activated and remain in operation until the end of discharge. After activation, the TEC and LC operate with an input current of 0.5 A and a mass flow rate of 0.1 g/s, respectively.

Figure 5A illustrates the variation curves of the maximum battery temperature and temperature difference when the operational strategy is applied during discharge. When this strategy is implemented, the T_{max} of the battery reaches 322.93 K, and the ΔT_{max} of the battery is 2.28 K. Compared with the case without the operational strategy, the T_{max} of the battery increases by 1.42 K but remains below 323.15 K, while the ΔT_{max} of the battery decreases

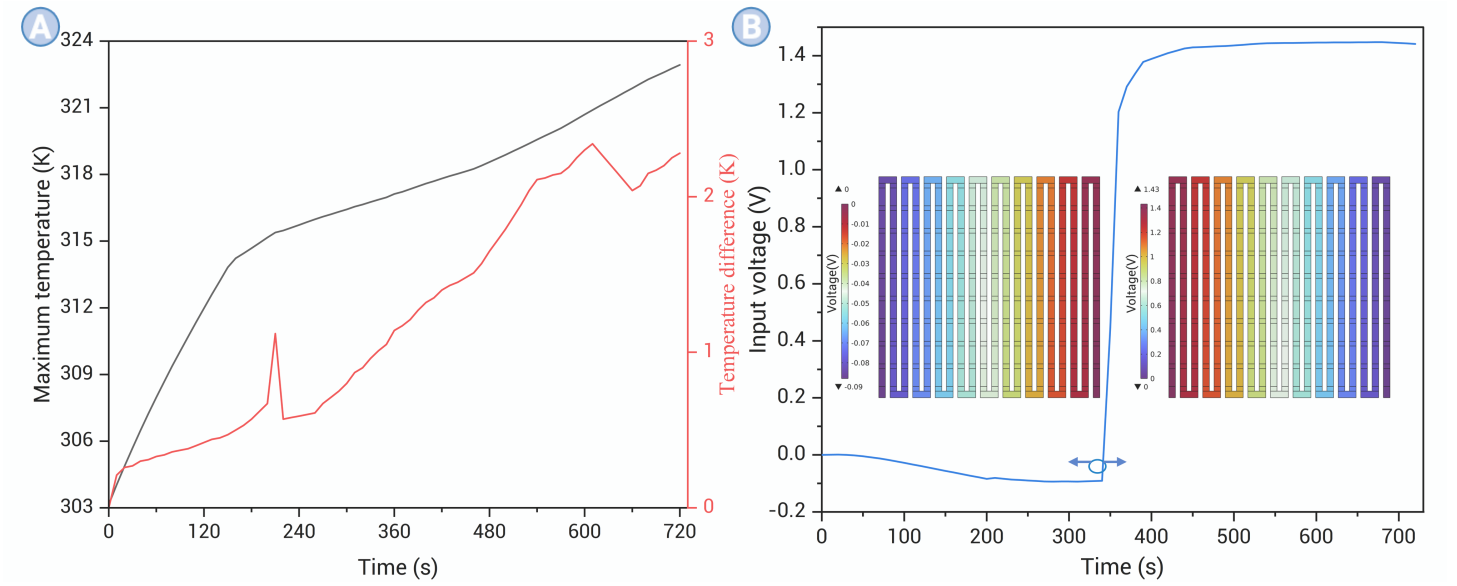

Figure 5. System performance after implementing the operational strategy: (A) Thermal performance of the system; (B) Input voltage of the TEG and its temperature distribution characteristics.

by 0.28 K. More importantly, the TEG power generation duration extends to 340 s, and the operation time of the active cooling system is reduced by 47.2%, significantly lowering system energy consumption. Figure 5B illustrates the variation and distribution characteristics of TEM input voltage during battery discharge. It can be observed that the polarity of the TEM voltage reverses before and after 340 s. Before 340 s, TEM functions as a TEG for power generation, exhibiting a negative voltage whose absolute value gradually increases, reaching a maximum of 0.093 V. This indicates that the temperature difference across the TEG increases as discharge progresses. After 340 s, TEM operates as a TEC to cool the battery, resulting in a positive voltage that sharply rises before stabilizing at 1.43 V. Additionally, the output voltage of the TEG is significantly lower than the input voltage of the TEC, indicating that the energy consumption of the TEC far exceeds the energy generated by the TEG. This operational strategy primarily achieves energy savings by reducing the active cooling system's runtime, with the TEG contributing a small amount of energy.

The impact of LC on the net energy of the system

Employing LC can lower the hot side temperature of the TEC, thereby reducing the ΔT between its hot and cold sides and decreasing energy consumption. However, the hot and cold sides of the TEG are opposite to those of the TEC, so using LC to lower the cold side temperature of the TEG can increase the ΔT. Theoretically, an increased ΔT between the TEG's hot and cold sides would enhance its output power.[33] It is important to note that LC itself consumes energy, and for practical engineering applications, the additional power generated by the TEG must exceed the energy consumed by the LC. This section calculates the net energy of the system under different discharge rates (1 C, 2 C, 3 C, 4 C) and varying mass flow rates (0-0.9 g/s). Under the selected battery discharge rates, only the passive cooling system is used for battery thermal management, and the TEM functions exclusively as the TEG throughout the discharge process.

Figure 6 presents the net energy of the system under different discharge rates and mass flow rates. Firstly, compared to the case without LC (0 g/s), employing LC indeed increases the system's net energy, confirming that enhancing the ΔT across the TEG can improve its output power. At a fixed discharge rate, as the liquid cooling mass flow rate increases, the ΔT between the hot and cold sides of the TEG grows, and the system's net output energy rises accordingly. However, when the mass flow rate increases further, the energy consumption of the liquid cooling system increases markedly, leading to a decline in net energy. Specifically, at discharge rates of 1 C, 2 C, 3 C, and 4 C, the peak net energy occurs at mass flow rates of 0.3 g/s, 0.5 g/s, 0.7 g/s, and 0.7 g/s, respectively, with corresponding values of 22.15 J, 52.24 J, 53.60 J, and 41.93 J. As the discharge rate increases,

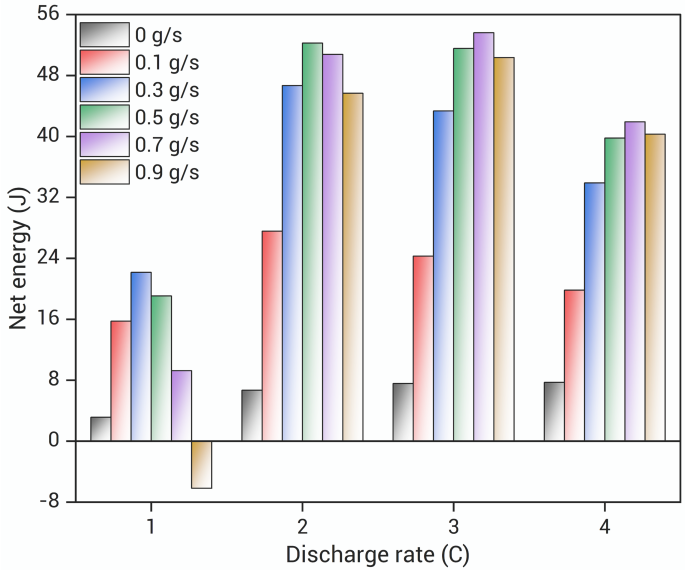

Figure 6. Net energy of the system under varying mass flow rates.

battery heat generation power rises, and a larger mass flow rate is typically required to increase the ΔT across the TEG and thus its power generation capability. Moreover, optimizing TEG performance via LC involves the dynamic coupling of battery heat release, PCM latent heat absorption, and LC heat removal, which causes the effects of different mass flow rates and discharge rates on system performance to differ significantly. Notably, at a 1C discharge rate, the mass flow rate should not exceed 0.7 g/s. Otherwise, for instance, at 0.9 g/s, the net energy of the system drops to −6.19 J, indicating that the additional power generated by the LC falls short of its energy consumption. In this case, even the TEG's power output is insufficient to offset the LC's consumption, necessitating additional energy input. Moreover, the discharge rate also affects the system's net energy, as manifested by the power generation duration and the initial ΔT (without optimized LC). When the mass flow rate is 0, increasing the discharge rate leads to higher system net energy, indicating a larger initial ΔT at higher discharge rates. Under fixed mass flow conditions, the system's net energy follows a parabolic trend with discharge rate-first increasing then decreasing-demonstrating that the increased ΔT is the primary driver of net energy gain, while the shortened generation time causes net energy to decline. Consequently, at discharge

rates of 2 C and 3 C, the system's net energy surpasses that observed at 1 C and 4 C.

CONCLUSIONS

This work, based on the hybrid BTMS integrating TEM, PCM, and LC, develops a multiphysics-coupled numerical model to evaluate the system's performance. During the battery discharge process, the TEM performs the dual functions of power generation and cooling, which not only meets the thermal management requirements but also enables waste heat recovery and reduces system energy consumption. The application scenarios of the TEG are clarified, an operational strategy for the active cooling system is proposed, and the system's net energy is improved after optimizing the mass flow rate. The main conclusions are as follows:

(1) The passive cooling system can meet the battery's cooling requirements at discharge rates from 1 C to 4 C, allowing the TEM to be used as the TEG for power generation. As the discharge rate increases, the ΔT between the TEG's hot and cold sides expands, thereby enhancing its output voltage and power.

(2) At a discharge rate of 5 C, using only the passive cooling system causes the battery's maximum temperature to exceed 323.15 K, thereby necessitating the introduction of an active cooling system. With the addition of the TEC, the T_{max} of the battery can be reduced to 322.3 K, and when LC and TEC are combined, the T_{max} and ΔT_{max} are further decreased to 321.51 K and 2.56 K, respectively. Moreover, cooling the TEC's hot side with LC improves its cooling efficiency, thereby reducing the system's input power.

(3) An operational strategy for the active cooling system is proposed: the active cooling system is activated when the battery temperature reaches the upper limit of the phase change temperature (at 340 s). This strategy not only meets the thermal management requirements but also allows the TEG to generate power within 340 s and reduces the active cooling system's operating time by 47.2%, thereby significantly lowering system energy consumption.

(4) Lowering the TEG's cold-side temperature via LC can effectively increase the temperature difference between its hot and cold sides, thereby enhancing output power. However, the mass flow rate must be controlled to prevent its energy consumption from exceeding the power generation gain of the TEG. The system's net energy initially increases and then decreases with rising mass flow rate, indicating the existence of an optimal mass flow rate (e.g., 0.3 g/s at 1C, 0.5 g/s at 2C, and 0.7 g/s at 3C and 4C). Excessively high flow rates (e.g., over 0.7 g/s at 1C) will result in negative net energy.

Nomenclature

Symbols

σ	electrical conductivity, $S \cdot m^{-1}$
c_p	specific heat, $J \cdot kg^{-1} \cdot K^{-1}$
D	diameter, mm
$\vec{E}$	electric field density vector, $V \cdot m^{-2}$
h	heat transfer coefficient, $W \cdot m^{-2} \cdot K^{-1}$
H	enthalpy, $J \cdot kg^{-1}$
I	current, A
$\vec{J}$	current density vector, $A \cdot m^{-2}$
k	thermal conductivity, $W \cdot m^{-1} \cdot K^{-1}$
L	latent enthalpy, $kJ \cdot kg^{-1}$
$\dot{m}$	mass flow rate, $g \cdot s^{-1}$
p	pressure, Pa
P	power, W
Q	heat generation rate, W
R	resistance,Ω
Re	Reynolds number
$\dot{S}$	energy source term
t	time, s
T	temperature, K
$\vec{V}$	velocity vector, $m \cdot s^{-1}$

Greek symbols

EV	electric vehicle
μ	dynamic viscosity, Pa·s
ρ	density, $kg \cdot m^{-3}$
α	Seebeck coefficient, $\mu V \cdot K^{-1}$
β	liquid fraction
φ	electrical potential, V

Subscripts

amb	ambient
b	battery
c	cold side
ce	ceramic plates
co	copper electrodes
h	hot side
inlet	the inlet of the coolant
l	liquid phase
n	n-type semiconductor
outlet	the outlet of the coolant
p	p-type semiconductor
PCM	phase change material
pump	the pump of liquid cooling
s	solid phase
x	name of different materials

Abbreviations

BTMS	battery thermal management system
HP	heat pipe
PCM	phase change material
TEC	thermoelectric cooler

REFERENCES

1. Murugan M., Saravanan A., Elumalai P.V., et al. (2022). Thermal management system of lithium-ion battery packs for electric vehicles: An insight based on bibliometric study. *J. Energy Storage* **52**:104723. DOI:10.1016/j.est.2022.104723
2. Zhou W., Li M., Zhang Q., et al. (2024). Potential and challenges of capacitive power transfer systems for wireless EV charging: A review of key technologies. *Green*

Energy Intell. Transp. **3**:100174. DOI:10.1016/j.geits.2024.100174
3. International Energy Agency. (2024). EV battery supply chain sustainability. *IEA*. https://www.iea.org/reports/ev-battery-supply-chain-sustainability.
4. Khoshvaght-Aliabadi M., Ghodrati P., Kang Y.T. (2025). Developing a novel battery thermal management system utilizing supercritical CO_2 as the cooling medium. *Appl. Energy* **381**:125207. DOI:10.1016/j.apenergy.2024.125207
5. Liu X., Wu P.Y., Su C.Q., et al. (2025). Research on precise temperature control performance of battery thermal management system integrating piezoelectric pump and thermoelectric cooler. *Energy* **317**:134623. DOI:10.1016/j.energy.2024.134623
6. Li H., Chen L., Zuo H., et al. (2024). Performance enhancement of a battery thermal management system using novel liquid cold plates with micro-channel featuring pin fins. *Energy* **301**:131731. DOI:10.1016/j.energy.2024.131731
7. Luo D., Jiang L., Wu Z., et al. (2025). Realizing cyclic utilization of phase change materials in thermoelectric-based battery thermal management system under real discharge–charge conditions. *J. Energy Storage* **114**:115682. DOI:10.1016/j.est.2025.115682
8. Li X. and Wang R. (2025). Towards integrated thermal management systems in battery electric vehicles: A review. *eTransportation* **24**:100396. DOI:10.1016/j.etran.2025.100396
9. Pilali E., Soltani M., Hatefi M., et al. (2025). Passive thermal management systems with phase change material-based methods for lithium-ion batteries: A state-of-the-art review. *J. Power Sources* **632**:236345. DOI:10.1016/j.jpowsour.2025.236345
10. Shahmohammadi M., Seddighi S., Taklifi A. (2024). Active and hybrid battery thermal management system using microchannels and phase change materials for efficient energy storage. *J. Power Sources* **621**:235317. DOI:10.1016/j.jpowsour.2024.235317
11. Murali G., Sravya G.S.N., Jaya J., et al. (2021). A review on hybrid thermal management of battery packs and cooling performance by enhanced PCM. *Renew. Sustain. Energy Rev.* **150**:111513. DOI:10.1016/j.rser.2021.111513
12. Li Y., Zhang R., Zhou B., et al. (2025). One-pot strategy for multifunctional recyclable thermally conductive phase change composites toward efficient thermal management. *Chem. Eng. J.* **521**:166972. DOI:10.1016/j.cej.2025.166972
13. Ping P., Dai X., Kong D., et al. (2023). Experimental study on nano-encapsulated inorganic phase change material for lithium-ion battery thermal management and thermal runaway suppression. *Chem. Eng. J.* **463**:142401. DOI:10.1016/j.cej.2023.142401
14. Masthan Vali P.S.N., Murali G., Chinnasamy S. (2023). Comparison study on cooling management of composite phase change material battery pack. *Thermal Sci.* **27**:218–228. DOI:10.2298/TSCI220422218V
15. Abd H.M., Khalifa A.H.N., Hamad A.J. (2024). Experimental comparison of Li-ion battery thermal management systems using a hybrid flat heat pipe coupled with phase change materials. *J. Energy Storage* **84**:110963. DOI:10.1016/j.est.2024.110963
16. Kumar R. and Panigrahi P.K. (2024). A hybrid battery thermal management system using ionic wind and phase change material. *Appl. Energy* **359**:122676. DOI:10.1016/j.apenergy.2024.122676
17. Liu Z., Zhang X., Qi N. (2025). Performance analysis and multi-objective optimization of a hybrid thermal management system based on PCM and liquid cooling. *J. Energy Storage* **135**:118264. DOI:10.1016/j.est.2025.118264
18. Luo D., Wu Z., Chen H., et al. (2025). Thermal performance of an active battery thermal management system combining annular thermoelectric coolers and phase change materials. *Renew. Energy* **249**:123278. DOI:10.1016/j.renene.2024.123278
19. Luo D., Wu Z., Jiang L., et al. (2024). Rapid cooling and latent heat recovery in thermoelectric-based battery thermal management systems at high temperatures. *Appl. Energy* **370**:123642. DOI:10.1016/j.apenergy.2024.123642
20. Luo D., Chen H., Chen W.H., et al. (2025). Interdependent optimization strategies for material, module, and system designs in thermoelectric devices. *Device* **3**:100752. DOI:10.1016/j.device.2025.100752
21. Jiang L., Zhang H., Li J., Xia P. (2019). Thermal performance of cylindrical battery modules impregnated with PCM composites based on thermoelectric cooling. *Energy* **188**:116048. DOI:10.1016/j.energy.2019.116048
22. Wei J., Zhou Y., Wang Y., et al. (2023). Large-sized thermoelectric modules composed of cement-based composite blocks for pavement energy harvesting. *Energy* **265**:126398. DOI:10.1016/j.energy.2023.126398
23. Li Y., Chen Z., Feng Y., et al. (2023). A novel petal-type battery thermal management system with dual phase change materials. *Int. J. Heat Mass Transfer* **207**:123989. DOI:10.1016/j.ijheatmasstransfer.2023.123989
24. Chen H., Tang Y.F., Zhou Y.X., et al. (2023). Steady and transient sensitivity investigations on a passive battery thermal management system coupled with PCM and heat pipes. *J. Energy Storage* **73**:109054. DOI:10.1016/j.est.2023.109054
25. Hu Q., Luo D., Guo J., et al. (2022). Broad temperature plateau for high thermoelectric properties of n-type $Bi_2Te_{2.7}Se_{0.3}$ via defect engineering. *ACS Appl. Mater. Interfaces* **15**:1296–1304. DOI:10.1021/acsami.2c18645.
26. Mama M., Solai E., Capurso T., et al. (2025). Comprehensive review of multi-scale lithium-ion battery modeling: From electrochemical dynamics to thermal management. *Energy Convers. Manage.* **325**:119223. DOI:10.1016/j.enconman.2025.119223
27. Dwivedi A., Kumar R., Goel V., et al. (2025). Comprehensive review on heat pipe-assisted hybrid battery thermal management strategies. *J. Energy Storage* **112**:115475. DOI:10.1016/j.est.2025.115475
28. Wu C., Qiu C., Yuan X., et al. (2024). Numerical study and optimization of battery thermal management systems based on fin–PCM under variable gravity. *Appl. Therm. Eng.* **244**:122777. DOI:10.1016/j.applthermaleng.2024.122777
29. Luo D., Wu H., Cao J., et al. (2024). Numerical investigation of battery thermal management system integrated with vapor chamber and thermoelectric refrigeration. *J. Clean. Prod.* **434**:140089. DOI:10.1016/j.jclepro.2024.140089
30. Liu X., Zhang C.F., Zhou J.G., et al. (2022). Thermal performance of battery thermal management system using fins to enhance thermoelectric cooler and PCM coupling. *Appl. Energy* **322**:119503. DOI:10.1016/j.apenergy.2022.119503
31. Hu S., Wang S., Ma C., et al. (2022). A hybrid cooling method with low energy consumption for lithium-ion batteries under extreme conditions. *Energy Convers. Manage.* **266**:115831. DOI:10.1016/j.enconman.2022.115831
32. Luo D., Jiang L., Chen H., et al. (2025). Enhanced energy efficiency of hybrid battery thermal management systems via delay control of thermoelectric coolers. *Renew. Energy* **253**:123607. DOI:10.1016/j.renene.2025.123607
33. Du Y., Chen Y., Liu J., et al. (2024). Boosting thermoelectric generator performance with tandem radiative, evaporative, and phase change cooling. *Nano Energy* **128**:109909. DOI:10.1016/j.nanoen.2024.109909

FUNDING AND ACKNOWLEDGMENTS

This work was supported by the National Natural Science Foundation of China (52306017).

AUTHOR CONTRIBUTIONS

All authors contributed to the manuscript and approved the final version.

DECLARATION OF INTERESTS

The authors declare no competing interests.

DATA AND CODE AVAILABILITY

Data are available from the corresponding author upon reasonable request.